ACS OMEGA

Open Access

This article is licensed under CC-BY-NC-ND 4.0

http://pubs.acs.org/journal/acsodf

Article

Production of Large Specific Capacitance by Electrodes with Low Active Mass and Synergistic Mechanisms

Hsin-Jung Tsai, Yung-Kai Yang, Ping-Chun Chen, Yu-Hsiang Liao, and Wen-Kuang Hsu*

Cite This: *ACS Omega* 2024, 9, 3923−3930

Read Online

ACCESS | Metrics & More | Article Recommendations | Supporting Information

ABSTRACT: Decoration of vanadium nitride nanoparticles on carbon nanotubes creates electrodes with three different energy storage mechanisms that operate synergistically to give a high specific capacitance with a low active mass. Calculation and measurements further indicate the power and energy density to be as high as 10^5−10^6 W/kg and 10^2 Wh/kg, respectively. Particle attachment also greatly improves the capacitive coefficient, including ionic transmittance, charge transfer, porosity, and conductivity. Corrosion tests based on the Tafel method reveal the corrosion potential and current of electrodes as low as −0.721 V and 7.53×10^{-4} A, respectively.

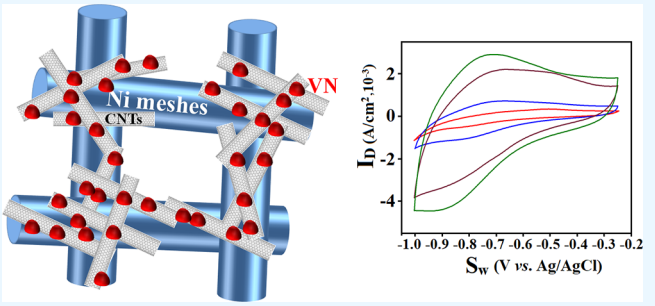

1. INTRODUCTION

Energy storage plays an important part in renewable energy systems and various devices have been developed such as thermochemical conversion,[1−3] mechanically driven type,[4,5] and electrochemical energy storage. Among others, energy storage through electrochemical mean prevails mainly due to its capability of producing high specific capacitance (C_s) and wide potential range.[6] Owing to their fast rate performance and high power density, the electrochemical capacitors (supercapacitors) have become the subject of great interest in the electrochemical society.[7,8] The study indicates two mechanisms involved in ionic absorption−desorption at electrode surfaces where the faradaic redox reaction (FROR) yields greater C_s than does the electric double-layer charging (EDLC).[9−13] Accordingly, a recent study focuses on transitional compounds with high oxidation states and electrical conductivity (σ), e.g., RuO_2,[14] V_6O_{13}/VO_2,[15] V_2O_5,[16] $CuCo_2O_4$,[17] Co_3N,[18] Ni_3N,[19] CrN,[20] VN, and their composites.[21,27] These, however, are often made in conjunction with plastic binders, thus significantly reducing the electrochemical performance. Carbon nanotubes (CNTs) are sp^2-bonded one-dimensional conductors and, similar to graphite and graphene, are also governed by EDLC.[28] Material hybridization has been proved to be efficient in improving the electrochemical performance of CNT-based electrodes, for example, composite electrodes made from homogeneous mixing of CNTs and VN. In this case, CNTs are added to improve σ, and energy storage mainly proceeds through VN-created FROR (**1**, Figure 1a).[29] Ion-intercalation mechanism (ITC), on the other hand, emerges as electrodes consist of core−shell nanostructures (i.e., VN-coated CNTs, **1** and **2**, Figure 1b).[30] Unlike conventional techniques that make electrochemical electrodes with large surface area and thickness,[31,32] this work, in contrast, tends to produce a large C_s on a low active mass as per the following; (i) an electrode made of thick active mass is indeed unnecessary since charge−discharge (i.e., redox reaction) takes place mainly at the surfaces;[33] (ii) a low active mass electrode means a reduced resistance, which is important in terms of power density.[8,9] This goal may be achieved by decorating VN nanoparticles on CNTs where three mechanisms synergistically operate to give a large amount of C_s (**1**, **2**, and **3**, Figure 1c). Measurements confirm a large C_s production and further indicate that the attached VN nanoparticles greatly promote the electrochemical

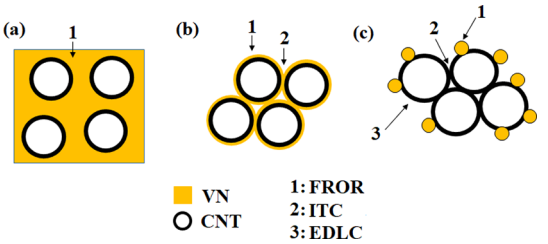

Figure 1. Three types of electrochemical electrodes. Electrode with FROR (**1**) arising from VN (a). Electrode with FROR (**1**) from VN and ITC (**2**) from the grooves between VN-coated CNTs (b). Electrode with FROR (**1**) from VN particles, ITC (**2**) from grooves between CNTs, and EDLC (**3**) from CNT surfaces (c).

Received: October 22, 2023
Revised: December 22, 2023
Accepted: December 29, 2023
Published: January 9, 2024

© 2024 The Authors. Published by American Chemical Society

activities of CNTs, including ionic transmittance, charge transfer, porosity, and σ. Comparison is also made on pure VN electrodes.

2. EXPERIMENTAL SECTION

Electrodes with hydrophilicity are of importance because FROR and EDLC operate on the basis of good wetting at the solid−liquid interface. Multiwalled CNTs made by metal catalytic pyrolysis of hydrocarbons (purity >90%, L-MWCNT1020, CONJUTEK, Taiwan) are treated with concentrated acid (2 M HNO_3+H_2SO_4, 50 °C) to improve the tube wetting and dispersion in aqueous solution.[34] The synthetic procedures of electrodes are summarized in Figure 2a

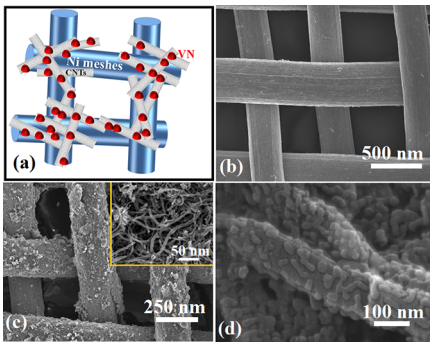

Figure 2. Fabrication of VN/CNTs/Ni electrodes (a). SEM images obtained from Ni net before CNT and VN coatings (b). CNT-coated Ni and highlighted image of CNTs (inset) (c), and the surface texture of VN/CNTs (d).

and are briefed as follows. Nickel (Ni) possesses a high resistance to corrosive solutions and is therefore used as a current collector.[35] A Ni net (spacing = 20 mm, 5 × 5 cm, 6N, 300 mesh, twill weave) is dipped into a CNT suspension made by ultrasonically dispersing treated CNTs (100 mg) in Mg $(NO_3)_2{\cdot}6H_2O$ (17 mg) dissolved in methanol (200 mL). The Ni net is electrified to electrophoretically transfer CNTs to metal surfaces (current = 3−5 mA, voltage = 70 V, and treating time = 10 min),[36] and the amount of transferred CNTs is as low as 5−7 mg, as per the measurements by a microbalance. The CNT-coated Ni net is then immersed in V_2O_5 (Showa, 99.5%, 3 g) dispersed in H_2O_2 for xerogel coating (Sigma-Aldrich, 4.3 wt %, 250 mL, 40−80 °C).[37] The oxide-coated CNT-Ni electrode is rinsed with distilled water to remove excess of oxide gel, followed by heating in anhydrous ammonia atmosphere at 600 °C for 6 h of nitridation (i.e., V_2O_5 + 10/3 NH_3 → 2VN + 5H_2O+ 2/3N_2).[38,39] The resultant materials are hereafter defined as VN/CNTs/Ni_t, where the subscript t denotes the deposition time of xerogel and is set at 15 and 30 min respectively (i.e., VN/CNTs/Ni_{15} and VN/CNTs/Ni_{30}). CNT-free samples (i.e., VN/Ni_t) with a similar t and oxide content (<2%) are also made and tested for comparison. Capacitive coefficients are characterized by cyclic voltammetry (CV) as follows. VN/CNTs/Ni_t are used as working electrodes in conjunction with Pt-counter and Ag/AgCl-reference electrodes to measure redox potentials in two types of neutral electrolytes for comparison, i.e., 4 M $LiCl_{(aq)}$ and 1.6 M $LiCl_{(aq)}$ dissolved in C_2H_5OH defined as **el-A** and **-B**. It is worth mentioning that $LiCl_{(aq)}$ is a neutral solution with the standard electrode potential (E^o/V) as high as −3.04 ($Li \rightarrow Li^+ + e^-$) and is therefore used as an electrolyte.[33] Since electrolysis of water occurs as the charging potential exceeds 1 V, the scan window (S_w) and rate (S_r) are set at −1 to −0.25 V and 10−50 mV s^{-1} for **el-A**. **el-B**, on the other hand, has a lower σ and is therefore tested in a wider S_w (−1.75−0 V). Electrochemical impedance spectra (ECIS) of the working electrodes are recorded at 10 mHz−100 kHz (5 mV), and the obtained Nyquist plots (i.e., Z_{re}−Z_{im} profiles) are analyzed with View software to uncover equivalent circuits at solid−liquid interfaces, where Z_{re} and Z_{im} denote the real and imaginary parts of the diffusive impedance. The structures and chemical composition of electrodes are inspected by X-ray diffraction (XRD, Shimadzu 6000, Cu/Kα radiation source), Raman analysis (LABRAM HR 800 UV, He/Ne excitation source, λ = 632.8 nm), field-emission scanning electron microscopy (FE-SEM, Hitachi SU8010, 15 kV accelerating voltage), high-resolution transmission electron microscopy (HRTEM, JEOL ARM-200F) equipped with an energy-dispersive spectrometer (EDS), and X-ray photoelectron spectroscopy (XPS, PHI Quantera SXM, Al/Kα radiation source); the XPS profiles have been calibrated with XPSPEAK41 software, NIST database, and C 1s peak at 284.6 eV. The specific surface area (S_{BET}) is measured by the nitrogen adsorption (N_A) technique at 77 K (ASTM D3663-92).

3. RESULTS AND DISCUSSION

SEM inspections confirm the (i) deposition of CNTs onto Ni net and (ii) conversion of V_2O_5 into VN nanoparticles on CNTs (Figure 2b,c and insert, Figure 2c); the latter is further verified by enhanced SEM (Figure 2d), HRTEM images (Figure 3a−c), and EDS profiles, where C, O, V, and N are measured to be 25.9, 13.4, 38.3, and 22.4 wt % (Figure S1, Supporting Information).

Figure 3d shows the EDS mapping recorded from Figure 3c, where C, N, and V arise from CNT and VN, and O is due to residual oxides arising from coatings, as evident by different diameters, i.e., 40 nm for nitride and 50 nm for oxide (Figure 3d).

XRD data agree with those of TEM and EDS and show reflections arising from the crystallographic planes of CNT (002) (2θ = 26.3°) and cubic VN (111) (2θ = 37.6°), (200) (2θ = 43.7°), (220) (2θ = 63.7°), and (311) (2θ = 76.4°) (Figure 3e),[40] where VN formation is also verified by XPS peaks at 396.8 and 513.8 eV, corresponding to N 1s and V_2p^3 (Figure 3f−h).[23,31] Additional evidence in support of V_2O_5 → VN conversion comes from (i) a trace of oxides after 20 s Ar plasma cleaning, i.e., V^{3+}(curve 1, 515 eV), V^{4+} (curve 2, 516.3 eV), and V^{5+} (curve 3, 517.1 eV) (Figure 3g,h);[23] (ii) nitridation that created pyridinic-N at tube surfaces (398.6 eV, N 1s spectra, Figure 3f);[41] (iii) the V−N vibrations that induced Raman A_g (96, 194, 404, 525, and 992 cm^{-1}) and B_{1g} modes (40, 283, and 694 cm^{-1}) (Figure 4a).

However, the CNT structure remains unchanged upon V_2O_5 → VN conversion, as evident by the detection of D- (1330 cm^{-1}, A_{1g}) and G-bands (1576 cm^{-1}, E_{2g}) arising from the phonon scattering at zone boundaries and C−C bond vibrations. Again, the high ratio of D- to G-band intensity (I_D/I_G = 0.998) and hydrogen-bonded amorphous carbon profile (peak a) verify CNTs to be made by catalytic pyrolysis (Figure 4b).[42,43]

The study also reveals (i) $VN_M \propto t$ and (ii) $VN_{M(CNTs/Ni)} > VN_{M(Ni)}$, where VN_M denotes coating the mass of VN and is only 1/6−1/9 of the reported data.[25,28−33] (i) is consistent

https://doi.org/10.1021/acsomega.3c08313
ACS Omega 2024, 9, 3923−3930

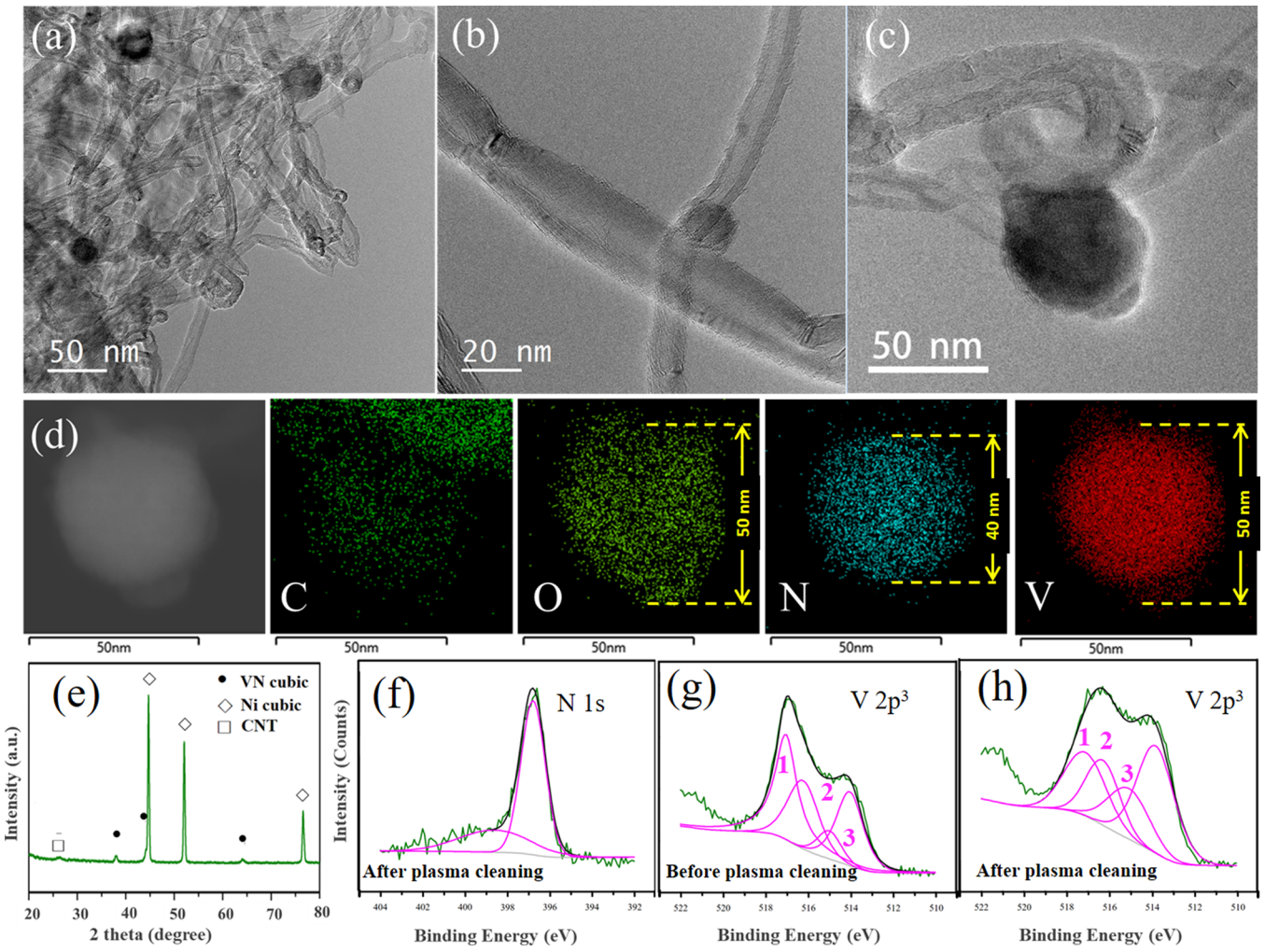

Figure 3. HRTEM images of VN particles on MWCNTs (a, c) and dark-field TEM images and the corresponding elemental mappings (d). XRD of VN/CNTs/Ni electrodes (e); XPS of N 1s (f) and V_2p^3 (g, h); deconvoluted curve 1 for V^{3+} (515 eV), curve 2 for V^{4+} (516.3 eV), and curve 3 for V^{5+} (517.1 eV).

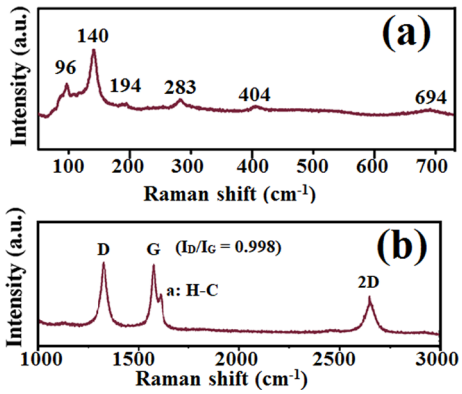

Figure 4. Raman spectra of VN (a) and CNTs (b). The peak a comes from hydrogen-bonded amorphous carbons (H−C).

with Table 1 and a report,[39] and (ii) indicates VN growth through oxygenated CNTs acting as templates.[36]

Figure 5a,b confirms the presence of oxygenated lattices in CNTs, where the content of carbonyl, hydroxyl, and carboxylic acid groups is 12.89, 8.54, and 9.8% based on the integration of XPS-C 1s and-O 1s spectra. In O 1s spectra, signals mainly come from VN and only ca. 10% for V_2O_5.[31]

Table 1. Content of C_{1s}, O_{1s}, and N_{1s} According to Deconvoluted XPS Spectra

sample	VN_M (mg/cm^2)
$VN/CNTs/Ni_{30}$	0.596 ± 0.02
$VN/CNTs/Ni_{15}$	0.267 ± 0.015
VN/Ni_{30}	0.337 ± 0.051
VN/Ni_{15}	0.0633 ± 0.003

Table 2 lists N_A and S_{BET} of $VN/CNTs/Ni_t$ and VN/Ni_t. Clearly, the coating of VN nanoparticles improves the electrode porosity, and improvement even reaches 2−3 orders of magnitude for $VN/CNTs/Ni_{15}$. The prolonged coating of VN nanoparticles however retards gas diffusion into micropores, so N_A and S_{BET} decrease, accounting for $N_{A(VN/CNTs/Ni15)} > N_{A(VN/CNTs/Ni30)}$ and $S_{BET(VN/CNTs/Ni15)} > S_{BET(VN/CNTs/Ni30)}$.[44]

Figure 6a presents the CV profiles obtained from **el-A** at S_r = 10 mV s^{-1} and S_w = −0.25 to −1 V. Apparently, profiles are asymmetric, and current density (I_D) follows the sequence $VN/CNTs/Ni_{30} > VN/CNTs/Ni_{15} > VN/Ni_{30} > VN/Ni_{15}$, attributable to the trapping of cations in VN particles.[45] Note that Ni current collector has a very low C_s (dark curve, Figures 6a and S3, Supporting Information).

https://doi.org/10.1021/acsomega.3c08313
ACS Omega 2024, 9, 3923−3930

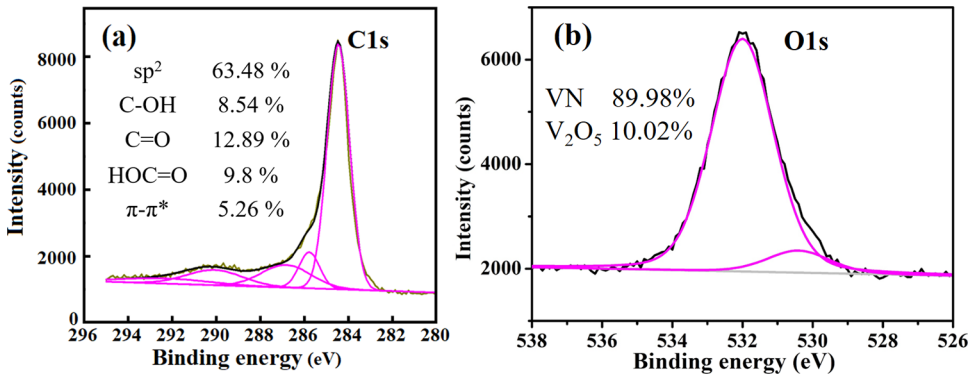

Figure 5. XPS of C 1s (a) and O 1s (b) after Ar plasma cleaning.

Table 2. N_A and S_{BET} of VN/CNTs/Ni$_t$ and VN/Ni$_t$

samples	N_A (cm^2/g)	S_{BET} (cm^2/g)
VN/CNTs/Ni$_{30}$	0.0816	0.3552
VN/CNTs/Ni$_{15}$	1.893	8.243
VN/Ni$_{30}$	0.0089	0.03884
VN/Ni$_{15}$	immeasurable	

Experiments carried out in **el-B** yield a similar result where two pairs of redox peaks at −0.59 and −1.35 V on positive and −0.53 and −1.3 V on negative potential arise from different S_w and solvation shells (Figure 6b).[25,26] We then calculate C_s as per equation $C_s = Q/\Delta V{\cdot}m$ (eq 1), where m is the mass of active materials (≈VN$_M$), ΔV is the working potential, and Q is charge (= half-integrated area of the CV curve divided by S_r).[11] Compared with the reported data, VN/CNTs/Ni$_{15}$ and VN/CNTs/Ni$_{30}$ exhibit a greater C_s; the former reaches a value as high as 511 F·g^{-1} in **el-A** and 468 F·g^{-1} in **el-B** (Figure 6c).[21−25] $C_{s(VN/CNTs/Ni15)} > C_{s(VN/CNTs/Ni30)}$ is consistent with Table 2 and again confirms that VN coating promoted N_A, S_{BET}, and C_s. VN/Ni, on the other hand, has limited N_A and S_{BET}, thus giving low C_s.

Figure 7a displays the C_s−S_r profiles of VN/CNTs/Ni$_{30}$ and VN/CNTs/Ni$_{15}$, where data points are extracted from $\mathbf{I_D}$−S_w plots (Figure S2, Supporting Information). Clearly, the profiles reveal $C_{s(VN/CNTs/Ni15)} > C_{s(VN/CNTs/Ni30)}$ and agree with the sequence $N_{A(VN/CNTs/Ni15)} > N_{A(VN/CNTs/Ni30)}$ and $S_{BET(VN/CNTs/Ni15)} > S_{BET(VN/CNTs/Ni30)}$, as observed in Table 2 and Figure 6c. $C_s \propto S_r^{-1}$ is indeed expected, since charge−discharge is time-dependent, and measurements give C_s = 69.2% for VN/CNTs/Ni$_{15}$ and 50.5% for VN/CNTs/Ni$_{30}$ at S_r = 50 mV s^{-1}. Note in the Helmholtz equation that C_s is inversely proportional to the diameter (**D**) of solvated ions $[M^+(H_2O)_n]$ at interfaces,[24] where ethanol hydrates with ions, thus resulting in a greater **D** [i.e., $M^+(CH_3CH_2OH)_n$] and C_s(**el-A**) > C_s(**el-B**) (Figure 7a).

Since FROR associates with chemical loss over repeated charge−discharge cycles, the retention experiments are therefore carried out in few hundreds of cycles.[38,39,46] Figure 7b shows C_s retention over 500 charge−discharge cycles at S_r = 20 mV s^{-1}, and profiles can be divided into two regions; the first lies in 1−150 cycles, where C_s decreases rapidly (Figure 7b). Profiles then level off in the second region (>150 cycles), with retention measured to be 54.6% (**el-A**) and 47.9% (**el-B**) for VN/CNTs/Ni$_{15}$ and 59% (**el-A**) and 76.9% (**el-B**) for VN/CNTs/Ni$_{30}$. The C_s decrease in the first region is due to the insertion of cations into VN lattices and VN oxidation; the former forms solid solution and is irreversible.[46] The latter produces surface roughness and holey structures (Figure 8a,b). It is worth mentioning that VN and V_2O_5 are nontoxic and can be recycled into metallurgy additives.[47−51]

$\mathbf{P_D}$ and $\mathbf{E_D}$ are important parameters widely used to justify the electrode performance and are expressed as $\mathbf{P_D} = V^2/4R_sm$ (eq 2) and $\mathbf{E_D} = C_sV^2/2$ (eq 3), where V corresponds to S_w, and R_s is the equivalent series resistance of the electrode and electrolyte. Table S1 (Supporting Information) lists $\mathbf{P_D}$ and $\mathbf{E_D}$ obtained from **el-A** and **-B** defined as $\mathbf{P_{D(el-A)}}$, $\mathbf{P_{D(el-B)}}$, $\mathbf{E_{D(el-A)}}$, and $\mathbf{E_{D(el-B)}}$. Apparently, both exceed the reported data ($\mathbf{P_D}$ = 104 W/kg and $\mathbf{E_D}$ = 10−20 Wh/kg)[52] and follow the sequences: (i) $\mathbf{P_{D(VN/Ni)}} > \mathbf{P_{D(VN/CNTs/Ni)}}$; (ii) $\mathbf{E_{D(VN/CNTs/Ni)}} > \mathbf{E_{D(VN/Ni)}}$; and (iii) $\mathbf{E_{D(el-A)}} < \mathbf{E_{D(el-B)}}$. Equation 2 and Table 1 account for (i), and (iii) is due to $\mathbf{E_D} \propto S_w$.[52] (ii) again verifies that the VN coating improved N_A, S_{BET}, and C_s (Table 2 and Figure 6). ItFulate $\mathbf{P_D}$ and $\mathbf{E_D}$ as per report.[53,54] Table 3 lists the recalculated $\mathbf{P_D}$ and $\mathbf{E_D}$ values which exceed the reported data.[55−57]

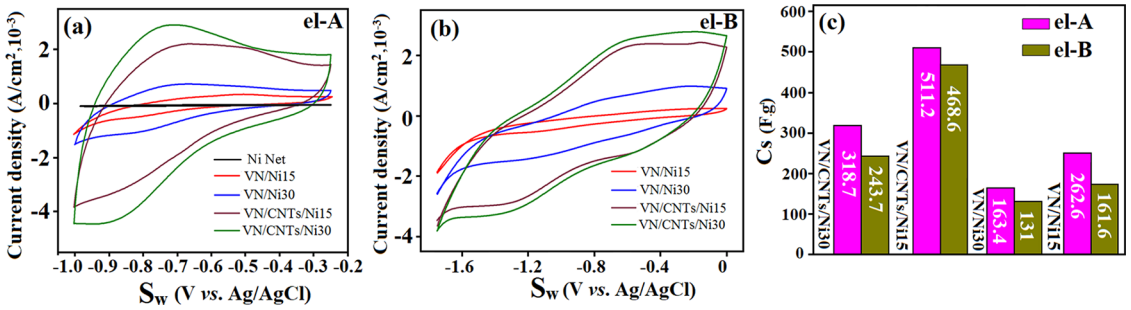

Figure 6. CV profiles of VN/Ni$_{15}$, VN/Ni$_{30}$, VN/CNTs/Ni$_{15}$, and VN/CNTs/Ni$_{30}$ obtained from **el-A** (a) and **el-B** (b) at 10 mV s^{-1}. C_s charts of VN/CNTs/Ni$_t$ and VN/Ni$_t$ obtained from **el-A** and **el-B** (c).

https://doi.org/10.1021/acsomega.3c08313
ACS Omega 2024, 9, 3923−3930

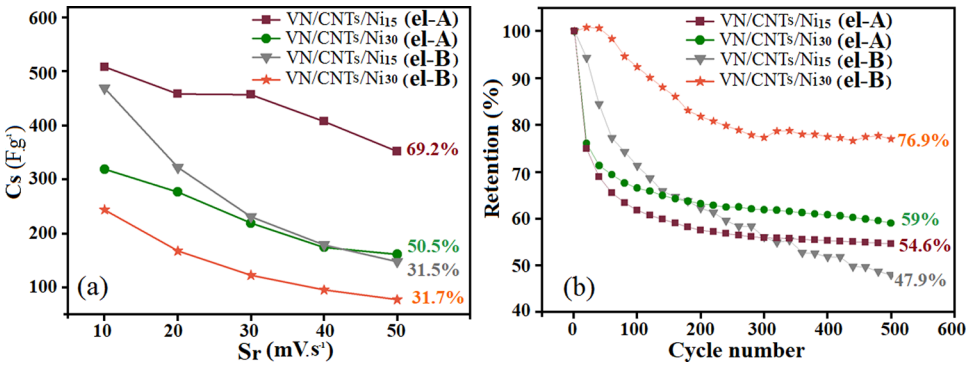

Figure 7. C_s−S_r (a) and C_s retention profiles (b) of VN/CNTs/Nit and VN/Nit in **el-A** and **el-B**.

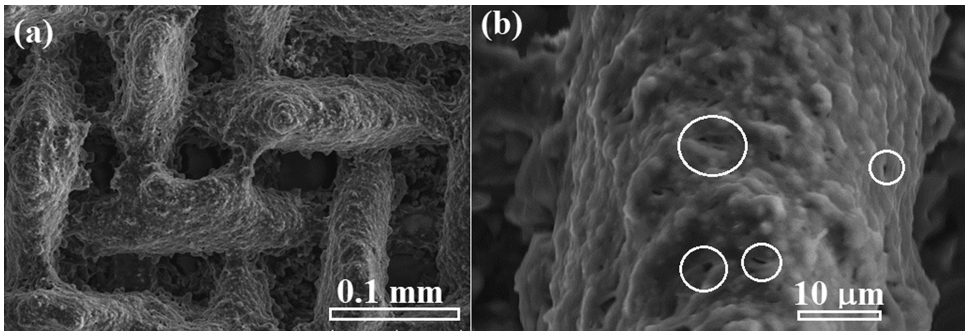

Figure 8. SEM images of used VN/CNTs/Ni_{15} electrodes (a) and a zoomed-in image where holey structures are circled (b).

Table 3. P_D and E_D of VN/CNTs/Ni_t and VN/Ni_t in el-A and el-B

samples	el-A		el-B	
	P_D (W/kg)	E_D (Wh/kg)	P_D (W/kg)	E_D (Wh/kg)
VN/CNTs/Ni_{15}	129600.1	25.56	10953.9	78.75
VN/CNTs/Ni_{30}	50066.1	15.94	44099	40.96
VN/Ni_{15}	609404.2	13.13	321158	27.16
VN/Ni_{30}	139672.1	8.17	31877.2	22.02

The ECIS values of VN/CNTs/Ni_t are analyzed on the basis of equivalent circuits that contain R_s, a parallel combination of constant phase element (CPE), diffusive resistance (R_d), charge-transfer resistance (R_{ct}), and double-layer capacitance (CPE_{dl}). CPE is calculated according to $Z_{CPE} = 1/T(i\omega)^P$ (eq 4), where T is the CPE constant (unit: $Fs^{(p-1)}$ cm^{-2}), ω is angular frequency, P is phase angle, and $P = 1$ represents an ideal capacitor.[57−59] Note that Warburg impedance is excluded from ECIS because it arises from the electrode bulk and cannot depict the diffusion of ions into nanostructures.[57] Table 4 lists the related parameters, and the Z_{re}−Z_{im} plots are shown in Figure 9a,b.

First, charge−discharge in **el-A** exhibits a time constant (semicircle) arising from the parallel combination of CPE_{dl} with R_s, R_{ct}, and R_d (insets, Figure 9a). Second, $R_{s(\textbf{el-A})} < R_{s(\textbf{el-B})}$ verifies a greater ionic conductivity in aqueous solution, the electrolyte conductivity being measured to be 60−65 m·S/cm for **el-A** and 11.6 m·S/cm for **el-B**. Third, $R_{ct(\textbf{el-A})} \ll R_{ct(\textbf{el-B})}$ indicates a greater ionic admittance in **el-A** (Table 4). Charge transfer in **el-B**, however, requires a greater activation energy across the double layer at the interface, so CPE_{dl}-T is low, and the Z_{re}−Z_{im} plot exhibits two time constants; the low-frequency one comes from the additional CPE connected in series with R_{ct} (blue circle, Figure 9b).[31,60] Fourth, the VN coating promotes CPE-T by 1−2 orders of magnitude.[61] Fifth, CPE_{dl}-P and CPE-P in **el-A** and **-B** are comparable. In other words, the increased C_s and $R_{d(VN/CNTs/Ni)} > R_{d(VN/Ni)}$ truly originate from VN coating that improved porosity, ion accessibility, charge transfer, and σ. In addition to C_s promotion, electrodes may corrode in polar electrolytes, thus

Table 4. Electrochemical Parameters of VN/CNTs/Ni and VN/Ni in el-A and el-B

el-A	R_S	CPE_{dl}-T	CPE_{dl}-P	R_{ct}	CPE-T	CPE-P	R_d
VN/CNTs/Ni_{15}	2.464	0.032	0.9924	3.803	0.044	0.798	516.2
VN/CNTs/Ni_{30}	2.921	0.032	0.981	3.539	0.04	0.770	501
VN/Ni_{15}	2.321	2×10^{-4}	0.945	2.694	1.5×10^{-3}	0.702	585.5
VN/Ni_{30}	2.255	1.1×10^{-3}	0.9715	4.234	5×10^{-3}	0.725	513
el-B	R_S	CPE_{dl}-T	CPE_{dl}-P	R_{ct}	CPE-T	CPE-P	R_d
VN/CNTs/Ni_{15}	10.47	1.34×10^{-5}	0.797	50.05	0.018	0.847	509
VN/CNTs/Ni_{30}	11.91	9.36×10^{-6}	0.847	48.15	0.018	0.835	555
VN/Ni_{15}	14.88	9.6×10^{-6}	0.818	52.82	5.2×10^{-4}	0.664	1145
VN/Ni_{30}	24.45	8.73×10^{-6}	0.883	48.24	1.45×10^{-3}	0.736	1141

https://doi.org/10.1021/acsomega.3c08313
ACS Omega 2024, 9, 3923−3930

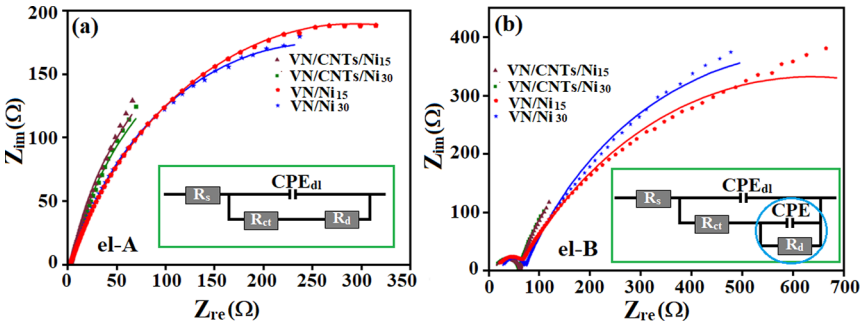

Figure 9. Z_{re}−Z_{im} plots of VN/CNTs/Ni_t and VN/Ni_t in **el-A** (a) and **el-B** (b); insets display the corresponding equivalent circuits. Circled part denotes the formation of additional CPE in **el-B,** which creates the second time constant at a low frequency.

reducing C_s and retention. Corrosion tests are carried out using the Tafel method, and the corrosion potential (V_{cor}) and current (I_{cor}) are measured at the linear region of the V_{cor}−logI_{ap} plot, where I_{ap} is applied current.[62] Extrapolation at the linear region (= 50 mV) gives V_{cor} = −0.721 and I_{cor} = 7.53 × 10^{-4} for Ni meshes, values which are low and approximate that of CNTs (V_{cor} = −0.735 and I_{cor} = 6.80 × 10^{-4}). Finally, it is important to give an estimate of the cost of electrode fabrication in comparison with the Li-ion battery systems (4−6 USD/Wh). Based on the current market price of related materials, the study here roughly lies on 2 USD/Wh and may be further reduced to 0.5−1 USD/Wh through mass production;[63] first, transfer of CNTs onto a Ni current collector and subsequent oxide deposition can be achieved in a large scale;[38,39] second, Figures 2 and 6 confirm the device reliability and reproducibility.

4. CONCLUSIONS

Since charge−discharge processes mainly take place at the solid−liquid interface, the fabrication of electrodes with thick active mass is therefore unnecessary. This study demonstrates the production of high C_s, $\mathbf{P_D}$, and $\mathbf{E_D}$ on a low active mass electrode where three different energy storage mechanisms synergistically operate. The VN/CNTs/Ni and VN/Ni electrodes are therefore made and tested in two different neutral electrolytes for comparison. The coating of VN nanoparticles onto CNTs significantly improves σ, N_A, S_{BET}, R_d, and C_s, and $C_{s(\mathbf{el\text{-}A})} > C_{s(\mathbf{el\text{-}B})}$ is due to lower R_s and R_{ct}. Prolonged coating of VN nanoparticles reduces N_A and S_{BET}, thus giving $C_{s(VN/CNTs/Ni15)} > C_{s(VN/CNTs/Ni30)}$. The V_{cor} and I_{cor} values of CNTs and Ni are very low and are −0.7 and 7 × 10^{-4}, respectively.

■ ASSOCIATED CONTENT

Data Availability Statement

Data will be made available on request.

Supporting Information

The Supporting Information is available free of charge at https://pubs.acs.org/doi/10.1021/acsomega.3c08313.

EDS profiles of VN, TEM images and CV profiles of VN/CNTs/Ni_{30} and VN/CNTs/Ni_{15} at different scan rates, power density and energy density of VN/CNTs/Ni and VN/Ni in **el-A** and **el-B**, and CV profile of the Ni current collector in **el-A** (PDF)

■ AUTHOR INFORMATION

Corresponding Author

Wen-Kuang Hsu − *Department of Materials Science and Engineering, National Tsin-Hua University, Hsinchu City 300044, Taiwan;* orcid.org/0000-0002-7034-1084; Phone: +886 3 5715131#35399; Email: wkhsu@mx.nthu.edu.tw

Authors

Hsin-Jung Tsai − *Department of Materials Science and Engineering, National Tsin-Hua University, Hsinchu City 300044, Taiwan;* orcid.org/0000-0003-3560-179X

Yung-Kai Yang − *Department of Materials Science and Engineering, National Tsin-Hua University, Hsinchu City 300044, Taiwan;* orcid.org/0000-0003-4422-8878

Ping-Chun Chen − *Department of Materials Science and Engineering, National Tsin-Hua University, Hsinchu City 300044, Taiwan;* orcid.org/0009-0001-8984-7667

Yu-Hsiang Liao − *Department of Materials Science and Engineering, National Tsin-Hua University, Hsinchu City 300044, Taiwan*

Complete contact information is available at: https://pubs.acs.org/10.1021/acsomega.3c08313

Author Contributions

All authors contributed equally to this work.

Notes

The authors declare no competing financial interest.

■ ACKNOWLEDGMENTS

The authors thank the Ministry of Science and Technology of Taiwan for the financial support (MOST- 110-2112-M-007-014). This work was also supported by High Entropy. Materials Center from The Featured Areas Research Centre Program within the framework of the Higher Education Sprout Project by the Ministry of Education (MOE) and from the Project NSTC 111-2634-F-007-008 by the National Science and Technology Council (NSTC) in Taiwan. The authors also acknowledge the use of F200 HRTEM and ARM200 C_s TEM systems which belong to Instrumentation Centre at NTHU under funding by the Ministry of Science and Technology (MOST), Taiwan.

■ REFERENCES

(1) Ali, H. M.; Rehman, T.-U.; Arıcı, M.; Said, Z.; Duraković, B.; Mohammed, H. I.; Kumar, R.; Rathod, M. K.; Buyukdagli, O.; Teggar, M. Advances in thermal energy storage: Fundamentals and applications. *Prog. Energy Combust. Sci.* **2024**, *100*, No. 101109.

https://doi.org/10.1021/acsomega.3c08313
ACS Omega 2024, 9, 3923−3930

(2) Pocha, C. K. R.; Chia, W. Y.; Silvanir; Kurniawan, T. A.; Khoo, K. S.; Chew, K. W. Thermochemical conversion of different biomass feedstocks into hydrogen for power plant electricity generation. *Fuel* **2023**, *340*, No. 127472.
(3) Raganati, F.; Ammendola, P. Review of Carbonate-Based Systems for Thermochemical Energy Storage for Concentrating Solar Power Applications: State-of-the-Art and Outlook. *Energy Fuels* **2023**, *37* (3), 1777−1808.
(4) Bolund, B.; Bernhoff, H.; Leijon, M. Flywheel energy and power storage systems. *Renewable and Sustainable Energy Reviews* **2007**, *11* (2), 235−258.
(5) Amiryar, M. E.; Pullen, K. R. A Review of Flywheel Energy Storage System Technologies and Their Applications. In *Applied Sciences*, **2017**; Vol. *7*, DOI: 286, .
(6) Kang, B.; Ceder, G. Battery materials for ultrafast charging and discharging. *Natur* **2009**, *458* (7235), 190−193.
(7) He, W.; Guo, W.; Wu, H.; Lin, L.; Liu, Q.; Han, X.; Xie, Q.; Liu, P.; Zheng, H.; Wang, L.; et al. Challenges and Recent Advances in High Capacity Li-Rich Cathode Materials for High Energy Density Lithium-Ion Batteries. *Adv. Mater.* **2021**, *33* (50), No. 2005937.
(8) Kötz, R.; Carlen, M. Principles and applications of electrochemical capacitors. *Electrochim. Acta* **2000**, *45* (15−16), 2483−2498.
(9) Wang, G.; Zhang, L.; Zhang, J. A review of electrode materials for electrochemical supercapacitors. *Chem. Soc. Rev.* **2012**, *41* (2), 797−828.
(10) Bose, S.; Kuila, T.; Mishra, A. K.; Rajasekar, R.; Kim, N. H.; Lee, J. H. Carbon-based nanostructured materials and their composites as supercapacitor electrodes. *J. Mater. Chem.* **2012**, *22* (3), 767−784.
(11) Sakata, Y.; Muto, A.; Uddin, M. A.; Yamada, N.; Marumo, C.; Ibaraki, S.; Kojima, K. Preparation of Carbon Electrodes for Electronic Double-Layer Capacitors by Carbonization of Metal-Ion-Exchanged Resins. *Electrochem. Solid-State Lett.* **2000**, *3* (1), 1−3.
(12) Hu, C.-C.; Chang, K.-H.; Lin, M.-C.; Wu, Y.-T. Design and Tailoring of the Nanotubular Arrayed Architecture of Hydrous RuO2 for Next Generation Supercapacitors. *Nano Lett.* **2006**, *6* (12), 2690−2695.
(13) Wu, M.-S.; Huang, C.-Y.; Lin, K.-H. Electrophoretic deposition of nickel oxide electrode for high-rate electrochemical capacitors. *J. Power Sources* **2009**, *186* (2), 557−564.
(14) Zheng, J. P.; Jow, T. R. A New Charge Storage Mechanism for Electrochemical Capacitors. *J. Electrochem. Soc.* **1995**, *142* (1), L6.
(15) Liu, Y.; Wu, X. High durable aqueous zinc ion batteries by synergistic effect of V6O13/VO2 electrode materials. *Journal of Energy Chemistry* **2023**, *87*, 334−341.
(16) Liu, Y.; Liu, Y.; Wu, X.; Cho, Y.-R. General Carbon Modification Avenue to Construct Highly Stable V2O5 Electrodes for Aqueous Zinc-Ion Batteries. *ACS Sustainable Chem. Eng.* **2023**, *11* (36), 13298−13305.
(17) Wang, X.; Sun, Y.; Zhang, W.-C.; Wu, X. Flexible CuCo2O4@Ni-Co-S hybrids as electrode materials for high-performance energy storage devices. *Chin. Chem. Lett.* **2023**, *34* (3), 107593.
(18) Fu, Z.-W.; Wang, Y.; Yue, X.-L.; Zhao, S.-L.; Qin, Q.-Z. Electrochemical Reactions of Lithium with Transition Metal Nitride Electrodes. *J. Phys. Chem. B* **2004**, *108* (7), 2236−2244.
(19) Wang, Y.; Fu, Z.-W.; Yue, X.-L.; Qin, Q.-Z. Electrochemical Reactivity Mechanism of Ni3 N with Lithium. *J. Electrochem. Soc.* **2004**, *151* (4), E162.
(20) Sun, Q.; Fu, Z.-W. An Anode Material of CrN for Lithium-Ion Batteries. *Electrochem. Solid-State Lett.* **2007**, *10* (8), A189.
(21) Cheng, F.; He, C.; Shu, D.; Chen, H.; Zhang, J.; Tang, S.; Finlow, D. E. Preparation of nanocrystalline VN by the melamine reduction of V2O5 xerogel and its supercapacitive behavior. *Mater. Chem. Phys.* **2011**, *131* (1−2), 268−273.
(22) Zhou, X.; Chen, H.; Shu, D.; He, C.; Nan, J. Study on the electrochemical behavior of vanadium nitride as a promising supercapacitor material. *J. Phys. Chem. Solids* **2009**, *70* (2), 495−500.
(23) Glushenkov, A. M.; Hulicova-Jurcakova, D.; Llewellyn, D.; Lu, G. Q.; Chen, Y. Structure and Capacitive Properties of Porous Nanocrystalline VN Prepared by Temperature-Programmed Ammonia Reduction of V2O5. *Chem. Mater.* **2010**, *22* (3), 914−921.
(24) Zhang, Y.; Feng, H.; Wu, X.; Wang, L.; Zhang, A.; Xia, T.; Dong, H.; Li, X.; Zhang, L. Progress of electrochemical capacitor electrode materials: A review. *Int. J. Hydrogen Energy* **2009**, *34* (11), 4889−4899.
(25) Zhao, X.; Sanchez, B. M.; Dobson, P. J.; Grant, P. S. The role of nanomaterials in redox-based supercapacitors for next generation energy storage devices. *Nanoscale* **2011**, *3* (3), 839−855.
(26) Fechler, N.; Tiruye, G. A.; Marcilla, R.; Antonietti, M. Vanadium nitride@N-doped carbon nanocomposites: tuning of pore structure and particle size through salt templating and its influence on supercapacitance in ionic liquid media. *RSC Adv.* **2014**, *4* (51), 26981−26989.
(27) Wang, G.; Hou, S.; Yan, C.; Zhang, X.; Dong, W. Preparation of three-dimensional vanadium nitride porous nanoribbon/graphene composite as an efficient electrode material for supercapacitors. *Journal of Materials Science: Materials in Electronics* **2018**, *29* (15), 13118−13124.
(28) Ghimbeu, C. M.; Raymundo-Pinero, E.; Fioux, P.; Beguin, F.; Vix-Guterl, C. Vanadium nitride/carbon nanotube nanocomposites as electrodes for supercapacitors. *J. Mater. Chem.* **2011**, *21* (35), 13268−13275.
(29) Xiao, X.; Peng, X.; Jin, H.; Li, T.; Zhang, C.; Gao, B.; Hu, B.; Huo, K.; Zhou, J. Supercapacitors: Freestanding Mesoporous VN/CNT Hybrid Electrodes for Flexible All-Solid-State Supercapacitors (Adv. *Mater. 36/2013). Adv. Mater.* **2013**, *25* (36), 4954−4954.
(30) Zhang, Q.; Wang, X.; Pan, Z.; Sun, J.; Zhao, J.; Zhang, J.; Zhang, C.; Tang, L.; Luo, J.; Song, B.; et al. Wrapping Aligned Carbon Nanotube Composite Sheets around Vanadium Nitride Nanowire Arrays for Asymmetric Coaxial Fiber-Shaped Supercapacitors with Ultrahigh Energy Density. *Nano Lett.* **2017**, *17* (4), 2719−2726.
(31) Zhang, L.; Holt, C. M. B.; Luber, E. J.; Olsen, B. C.; Wang, H.; Danaie, M.; Cui, X.; Tan, X.; Lui, V. W.; Kalisvaart, W. P.; et al. High Rate Electrochemical Capacitors from Three-Dimensional Arrays of Vanadium Nitride Functionalized Carbon Nanotubes. *J. Phys. Chem. C* **2011**, *115* (49), 24381−24393.
(32) Ji, J.; Li, Y.; Peng, W.; Zhang, G.; Zhang, F.; Fan, X. Advanced Graphene-Based Binder-Free Electrodes for High-Performance Energy Storage. *Adv. Mater.* **2015**, *27* (36), 5264−5279.
(33) Hong, M. S.; Lee, S. H.; Kim, S. W. Use of KCl Aqueous Electrolyte for 2 V Manganese Oxide/Activated Carbon Hybrid Capacitor. *Electrochem. Solid-State Lett.* **2002**, *5* (10), A227.
(34) Kuzmany, H.; Kukovecz, A.; Simon, F.; Holzweber, M.; Kramberger, C.; Pichler, T. Functionalization of carbon nanotubes. *Synth. Met.* **2004**, *141* (1), 113−122.
(35) Boccaccini, A. R.; Cho, J.; Roether, J. A.; Thomas, B. J. C.; Jane Minay, E.; Shaffer, M. S. P. Electrophoretic deposition of carbon nanotubes. *Carbon* **2006**, *44* (15), 3149−3160.
(36) Cho, J.; Konopka, K.; Rożniatowski, K.; García-Lecina, E.; Shaffer, M. S. P.; Boccaccini, A. R. Characterisation of carbon nanotube films deposited by electrophoretic deposition. *Carbon* **2009**, *47* (1), 58−67.
(37) Alonso, B.; Livage, J. Synthesis of Vanadium Oxide Gels from Peroxovanadic Acid Solutions: A 51V NMR Study. *J. Solid State Chem.* **1999**, *148* (1), 16−19.
(38) Kapoor, R.; Oyama, S. T. Synthesis of high surface area vanadium nitride. *J. Solid State Chem.* **1992**, *99* (2), 303−312.
(39) Kwon, H.; Choi, S.; Thompson, L. T. Vanadium Nitride Catalysts: Synthesis and Evaluation forn-Butane Dehydrogenation. *J. Catal.* **1999**, *184* (1), 236−246.
(40) Huang, K.; Bi, K.; Liang, C.; Lin, S.; Zhang, R.; Wang, W. J.; Tang, H. L.; Lei, M. Novel VN/C nanocomposites as methanol-tolerant oxygen reduction electrocatalyst in alkaline electrolyte. *Sci. Rep.* **2015**, *5*, 11351.
(41) Tung, F.-K.; Yoshimura, M.; Ueda, K. Direct Fabrication of Carbon Nanotubes STM Tips by Liquid Catalyst-Assisted Microwave Plasma-Enhanced Chemical Vapor Deposition. *J. Nanomater.* **2009**, *2009*, No. 612549.

https://doi.org/10.1021/acsomega.3c08313
ACS Omega 2024, 9, 3923−3930

(42) Zhou, B.; He, D. Raman spectrum of vanadium pentoxide from density-functional perturbation theory. *J. Raman Spectrosc.* **2008**, *39* (10), 1475−1481.
(43) Bokobza, L.; Zhang, J. Raman spectroscopic characterization of multiwall carbon nanotubes and of composites. *Express Polymer Letters* **2012**, *6* (7), 601−608.
(44) Madan, R. L.; S, C. S. G. *Physical Chemistry*; S. Chand & Company Limited, 2005.
(45) Lu, X.; Yu, M.; Zhai, T.; Wang, G.; Xie, S.; Liu, T.; Liang, C.; Tong, Y.; Li, Y. J. N. l.High energy density asymmetric quasi-solid-state supercapacitor based on porous vanadium nitride nanowire anode **2013**, *13*(6), 2628−2633, DOI: 10.1021/nl400760a.
(46) Djire, A.; Pande, P.; Deb, A.; Siegel, J. B.; Ajenifujah, O. T.; He, L.; Sleightholme, A. E.; Rasmussen, P. G.; Thompson, L. T. Unveiling the pseudocapacitive charge storage mechanisms of nanostructured vanadium nitrides using in-situ analyses. *Nano Energy* **2019**, *60*, 72−81.
(47) Fadel, T. R.; Steevens, J. A.; Thomas, T. A.; Linkov, I. The challenges of nanotechnology risk management. *Nano Today* **2015**, *10* (1), 6−10.
(48) Wu, Y.-D.; Zhang, G.-H.; Chou, K.-C. A Novel Process to Synthesize High-Quality Ferrovanadium Nitride. *Metallurgical and Materials Transactions B* **2016**, *47* (6), 3405−3412.
(49) Kim, H. S.; Kim, M.; Park, W.-K.; Yang, W.-G.; Nayak, M.; Shin, H. H.; Cho, K.; Kim, D.; Oda, T. Microalgae as an Effective Recovery Agent for Vanadium in Aquatic Environment. *Energies* **2022**, *15*, 4467 DOI: 10.3390/en15124467.
(50) Bhattacharya, G.; Fishlock, S. J.; McLaughlin, J. A.; Roy, S. S. Metal-oxide nanomaterials recycled from E-waste and metal industries: A concise review of applications in energy storage, catalysis, and sensing. *IJER* **2021**, *45* (5), 8091−8102.
(51) Du, L. Y.; Lin, H. J.; Ma, Z. Y.; Wang, Q. Q.; Li, D. S.; Shen, Y.; Zhang, W. N.; Rui, K.; Zhu, J. X.; Huang, W. Using and recycling V2O5as high performance anode materials for sustainable lithium ion battery. *J. Power Sources* **2019**, *424*, 158−164.
(52) Deng, W.; Ji, X.; Chen, Q.; Banks, C. E. Electrochemical capacitors utilising transition metal oxides: an update of recent developments. *RSC Adv.* **2011**, *1* (7), 1171−1178.
(53) Gogotsi, Y.; Simon, P. True Performance Metrics in Electrochemical Energy Storage. *Science* **2011**, *334* (6058), 917−918.
(54) Qu, D.; Shi, H. Studies of activated carbons used in double-layer capacitors. *J. Power Sources* **1998**, *74* (1), 99−107.
(55) Yue, Y.; Han, P.; Dong, S.; Zhang, K.; Zhang, C.; Shang, C.; Cui, G. Nanostructured transition metal nitride composites as energy storage material. *Chin. Sci. Bull.* **2012**, *57* (32), 4111−4118.
(56) Liu, Y.; Wu, Q.; Liu, L.; Manasa, P.; Kang, L.; Ran, F. Vanadium nitride for aqueous supercapacitors: a topic review. *Journal of Materials Chemistry A* **2020**, *8* (17), 8218−8233.
(57) Randles, J. E. B. Kinetics of rapid electrode reactions. *Discuss. Faraday Soc.* **1947**, *1* (0), 11−19.
(58) Engstrom, A. M.; Doyle, F. M. Exploring the cycle behavior of electrodeposited vanadium oxide electrochemical capacitor electrodes in various aqueous environments. *J. Power Sources* **2013**, *228*, 120−131.
(59) Hrdy, R.; Kynclova, H.; Drbohlavova, J.; Svatos, V.; Chomoucka, J.; Prasek, J.; Businova, P.; Pekarek, J.; Trnkova, L.; Kizek, R.; et al. Electrochemical Impedance Spectroscopy Behaviour of Guanine on Nanostructured Planar Electrode. *Int. J. Electrochem. Sci.* **2013**, *8* (4), 4384−4396.
(60) Perera, S. D.; Patel, B.; Nijem, N.; Roodenko, K.; Seitz, O.; Ferraris, J. P.; Chabal, Y. J.; Balkus, K. J. Vanadium Oxide Nanowire−Carbon Nanotube Binder-Free Flexible Electrodes for Supercapacitors **2011**, *1*(5), 936−945, DOI: 10.1002/aenm.201100221.
(61) Rahman, M. M.; Wang, J.-Z.; Idris, N. H.; Chen, Z.; Liu, H. Enhanced lithium storage in a VO2(B)-multiwall carbon nanotube microsheet composite prepared via an in situ hydrothermal process. *Electrochim. Acta* **2010**, *56* (2), 693−699.
(62) Noor, N.; Othman, R.; Hatta, M. M.; Ani, M. H. *Determination of Linear Tafel Region from Piecewise Linear Regression Analysis*, 2014; Vol. *2*; pp 22−27.
(63) Schmidt, O.; Hawkes, A.; Gambhir, A.; Staffell, I. The future cost of electrical energy storage based on experience rates. *Nat. Energy* **2017**, *2* (8), 17110.

https://doi.org/10.1021/acsomega.3c08313
ACS Omega 2024, 9, 3923−3930